Ocean Engineering 313 (2024) 119652

Contents lists available at ScienceDirect

Ocean Engineering

journal homepage: www.elsevier.com/locate/oceaneng

Research paper

# Hyperelastic behaviour of elastomers for wave energy applications

Guillermo Idarraga [a], Liu Yang [a,*], Farhad Abad [b], Yang Huang [b], Saishuai Dai [b], Qing Xiao [b], Saeid Lotfian [b], Feargal Brennan [b]

[a] Department of Mechanical and Aerospace Engineering, University of Strathclyde, 75 Montrose Street, Glasgow, G1 1XJ, UK
[b] Department of Naval Architecture, Ocean and Marine Engineering, University of Strathclyde, Glasgow, UK

ARTICLE INFO

*Keywords:*
Elastomers
Mechanical testing
Hyperelastic modelling
Oscillating water column
Flexible wave energy converter

ABSTRACT

Elastomers are increasingly recognized as a pivotal technology for realizing flexible wave energy converters (fWEC), owing to their elasticity, stretchability, and resilience to harsh marine environments. As a result, they frequently appear as a choice of material in modelling the behaviour of fWEC. This study undertakes the characterization of five different elastomers under varying loading conditions, including uniaxial, planar and biaxial tests. The hyperelastic behaviour of the materials was evaluated by implementing hyperelastic modelling, obtaining the hyperelastic constants for each elastomer. To validate these constants for fWEC application, experimental tests are conducted using an oscillating water column setup. These experiments offer insights into elastomeric membrane deformation under wave-induced conditions within a water tank. The resultant data is then compared with outcomes from a numerical model utilizing the established hyperelastic constants. Remarkably, the model accurately replicates the membrane deformation trends observed in the water tank experiments.

## 1. Introduction

According to the International Energy Agency, approximately 29% of global electricity generation was renewable in 2020. To achieve net-zero emissions by 2050, renewable power needs to expand and reach 60% of electricity generation by 2030. This would require an annual increment of 12%, double the current growth rate. To meet this goal, the annual power generation would need to rise from 134 GW in 2020 to 630 GW in 2030, demanding considerable effort (Bojek and Bahar, 2021; Lindquist, 2017). Oceans cover approximately 75% of the earth's surface and have the potential to supply 10–20% of the world's energy demand (Aderinto and Li, 2018), making them one of the most promising options for harvesting the required energy.

Unlike other renewable energy technologies such as solar or wind, wave energy is yet to achieve its global adaptation and continuing techno-economic development is required to facilitate the commercialisation of wave energy devices (Seanergy. Ocean Energies, 2016). Addressing various issues such as device survivability, maintenance, fatigue life, device mass and complex shapes is crucial to enhancing the reliability and cost-effectiveness of wave energy converters (WEC) (Materials Landscaping Study – Final Report). The marine environment poses unique and dynamic challenges for WEC, including enduring storms, continual wetting/drying cycles, intense solar radiation and exposure to salt-saturated water. Consequently, manufacturers historically relied on rigid materials such as concrete and metals, which, though durable, have proven problematic due to their weight, logistics, and manufacturing costs (Koca et al.; Collins, 2021). Additionally, metallic machinery exhibits poor compliance to wave conditions, resulting in load concentrations, premature failures due to fatigue, and corrosive damage (Yemm et al., 2012; Lin et al., 2015). Often, designs are excessively robust to address reliability concerns, resulting in poor cost-effectiveness.

Given the challenges of generating electricity using wave energy, there has been a noticeable shift towards fWEC. These designs prioritize flexibility, demonstrating superior adaptability to the dynamic sea conditions compared to conventional WEC, featuring innovative single-body structures with fewer parts and joints (Orphin et al., 2017; Alam, 2012; Kurniawan et al., 2017; Babarit et al., 2017). The characteristics of fWEC contribute to increased reliability, fatigue life, survivability, and reduced logistic costs due to their lighter-weight structures (Jean et al., 2012; Technology Description and Status Electric Eel; Chaplin et al., 2012).

Recent research has shown promising results in integrating the flexible body with the power generator using dielectric elastomers

* Corresponding author.
*E-mail address:* l.yang@strath.ac.uk (L. Yang).

https://doi.org/10.1016/j.oceaneng.2024.119652
Received 25 April 2024; Received in revised form 10 October 2024; Accepted 27 October 2024
Available online 31 October 2024

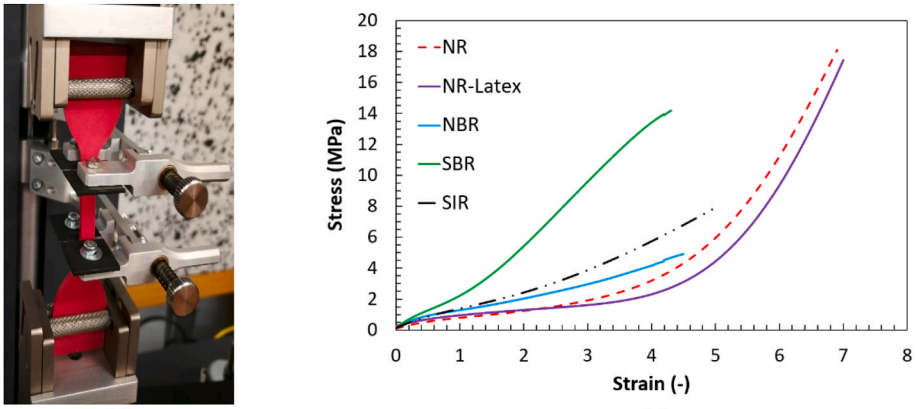


**Fig. 1.** (a) Photo of the experimental setup for uniaxial test (b) Typical uniaxial elastomers stress-strain curves.

(DEGs) (Collins, 2021; Jean et al., 2012; Moretti et al., 2020; Maas and Graf, 2012). Elastomers, like silicones, acrylics, and natural rubbers, have appeared in recent fWEC designs, offering advantages such as damping coefficient, fatigue life and high elongation, enhancing survivability, however, they have reduced stiffness and tensile strength. Moretti et al. (Moretti et al., 2020; Moretti et al.), introduce a novel fWEC based on an oscillating water column (OWC) architecture that utilises DEGs as a power take-off system. The wave-induced water motion drives air pressure oscillations inside the OWC that are converted into electrical energy using a circular diaphragm DEG at the top of the device. Moretti et al. implemented a VHB 4905 acrylic elastomer sandwiched between two carbon grease electrodes and a hyperelastic Mooney–Rivlin model was used to describe the material. When this elastomeric material is mechanically stretched by the increment in the pressure, the distance between the electrodes changes, leading to a variation in the device's capacitance. In the process, a high-voltage electric field is applied across the dielectric elastomer. As the elastomer stretches, the capacitance increases, and as it contracts, the capacitance decreases. When the capacitance decreases, if the voltage is maintained, the energy stored in the system increases rather than decreases, allowing mechanical energy to be converted into electrical energy. The energy conversion is achieved by controlling the charge and voltage on the dielectric layers during the deformation cycle. According to Moretti et al. (2019), a peak power output of up to 3.8 W was generated from the small-scale OWC prototype.

Despite their common use in marine structures, the selection and mechanical characterization of elastomers in fWEC applications have not been extensively explored. Developing a robust methodology for characterisation and modelling of elastomers for fWEC enables a better understanding and design of wave energy devices. Material properties play a crucial role in analysing the structural integrity, deformation, and power generation of fWEC (McDonald et al., 2019; Li et al., 2021). The reliability of device modelling is affected by the validity of the hyperelastic model applied to predict the elastomer behaviour and the test data quality used to describe the selected model.

The elastomers were chosen, and the mechanical response was characterised under conditions of plane stress (uniaxial tests), plane strain (planar tests), and equi-biaxial stress (biaxial tests). The results of the tests were then used to assess and determine suitable hyperelastic models using Abaqus software. Given most of the literature work on fWEC only provides very limited data on the material properties, the outcomes of this study can significantly contribute to the analysis of fWEC by providing more comprehensive experimental data and hyperelastic models of elastomers.

## 2. Materials

Natural rubber (NR), styrene-butadiene rubber (SBR), nitrile-butadiene rubber (NBR) and silicone rubber (SIR) used in this work were purchased from Coruba UK and latex rubber (NR-Latex) was supplied by PAR Group UK. It is worth noting that both SIR and latex rubber have been used in fWEC design for power generation (Ahamed et al., 2020; Righi et al., 2021; PolyWEC project; Kaltseis et al., 2014). The nominal thickness of all rubber samples is 3 mm, except for the latex rubber, whose nominal thickness is 0.38 mm.

## 3. Mechanical characterisation

The chosen elastomers underwent assessment under uniaxial, planar, and biaxial conditions to analyse their stress and strain responses and derive the hyperelastic constants. All evaluations were performed using a universal servo-electric test machine Testometric 500X-50 equipped with a calibrated 50 kN load cell.

### 3.1. Uniaxial loading

Uniaxial tests were performed on dumbbell-shaped specimens fabricated following ASTM D412/ISO 37 standards. Each elastomer was subjected to evaluation using a minimum of five samples. Sample displacement during the tests was measured using self-tightening grips and a long-range extensometer, as depicted in Fig. 1(a). The experiments were conducted at ambient temperature, employing a consistent cross-head speed of 100 mm/min until the elastomers failed, except for NR and NR-Latex samples, which reached the displacement limit of the machine without exhibiting any signs of failure.

Fig. 1(b) presents typical stress-strain curves obtained from the uniaxial tests with all five elastomers. For NBR, SBR, and SIR, this means material strength, which is not the case for NR and NR-Latex due to machine limitations. Notably, SBR exhibited significantly higher stiffness compared to other elastomers. This difference can be attributed to its more complex chemical structure, particularly the presence of the benzene group in the styrene, which hinders chain rotation, uncoiling, disentangling, and deformation through viscous flow under stress. On the other hand, elastomers with more linear chemical structures, such as NR, allow chains to rotate and slide more easily under stress, resulting in reduced stiffness under low and medium deformations. NR and NR-Latex exhibited a similar mechanical response in tension, with stiffness increasing after 400% of strain due to strain crystallisation, wherein molecules become more aligned with the load during deformation. This characteristic of natural rubbers allows them to achieve higher strength.

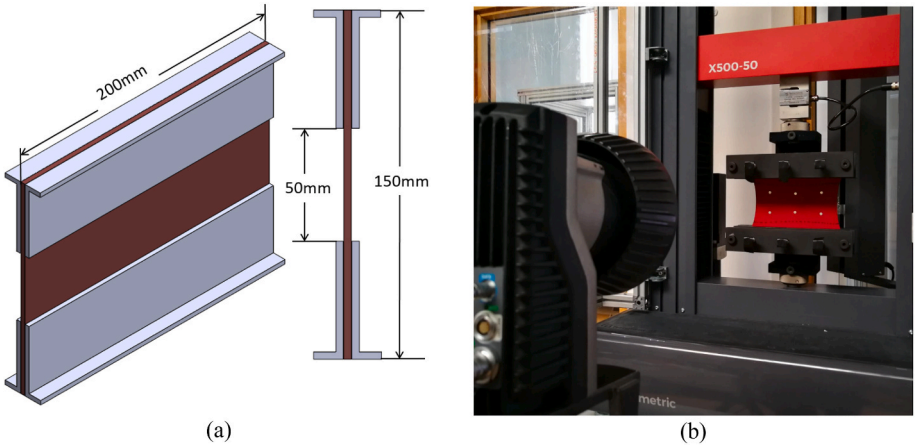


**Fig. 2.** (a) Schematic configuration of the metallic brackets and specimen, (b) photo of the experimental setup for planar tests with Qualisys optical measurement system.

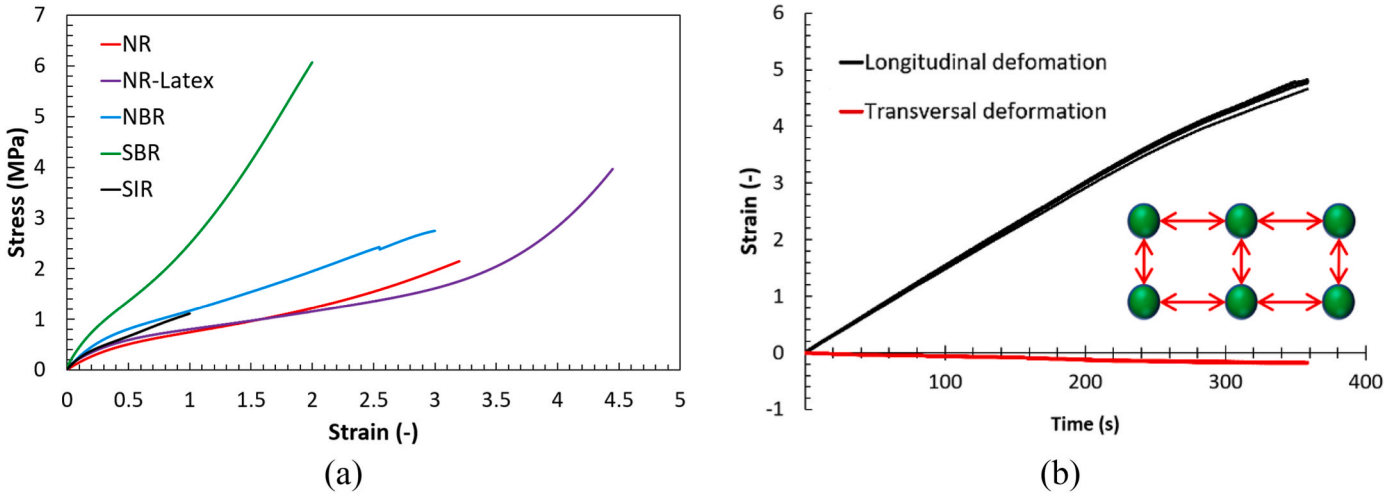


**Fig. 3.** (a) Elastomers stress-strain curves under planar loading conditions, (b) longitudinal and transverse displacement for NR-Latex.

### 3.2. Planar loading

The planar tension test involves subjecting a test sample to plane strain conditions, aiming to minimize or eliminate the effects of lateral strains. In this study, rectangular-shaped samples measuring 200 mm in width with a grip separation of 50 mm were employed. The samples were glued to L-shaped metal brackets using structural adhesive as shown in Fig. 2(a). The brackets also contribute to ensuring plane strain state by minimising transverse contraction of the samples during longitudinal loading. A consistent crosshead speed of 50 mm/min was

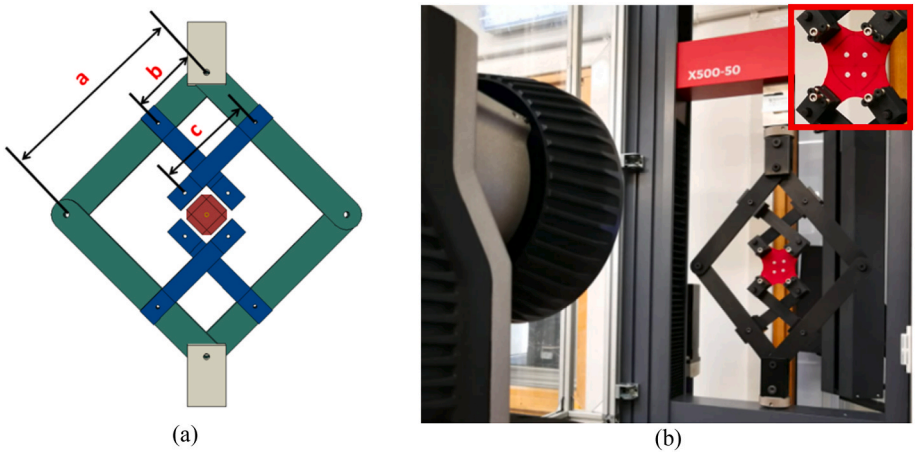


**Fig. 4.** (a) Schematic design of biaxial scissor arm, (b) photo of the experimental setup for biaxial tests with Qualisys optical measurement system.

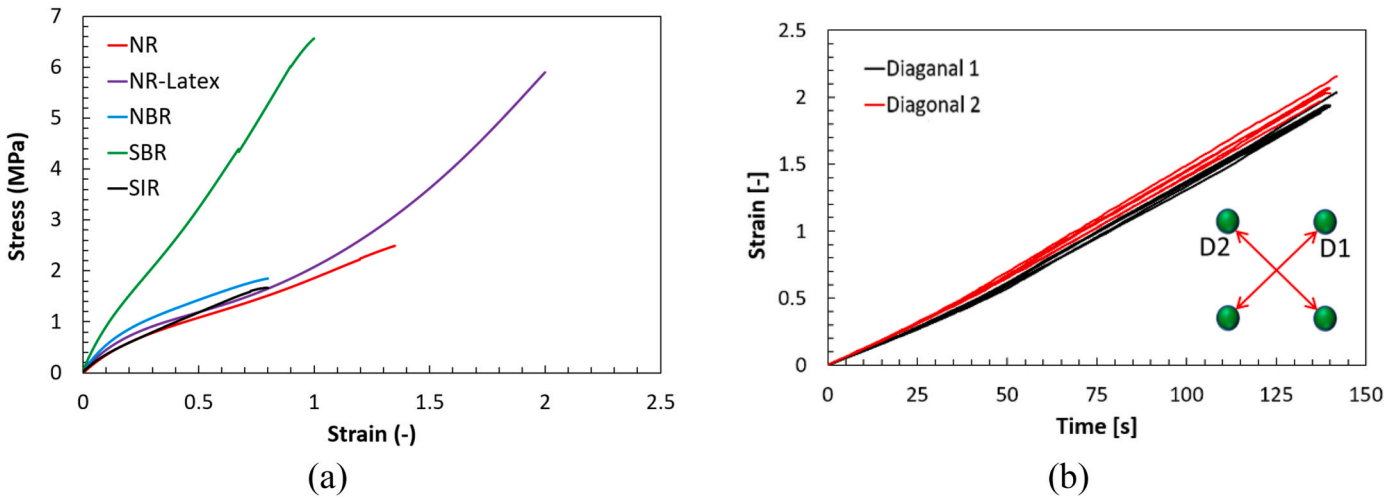


**Fig. 5.** (a) Elastomers stress-strain curves in biaxial test, (b) strains along the principal diagonal for NR-Latex.

maintained throughout the tests.

Due to the dimensions of the samples, it was not possible to implement the same extensometer used for the uniaxial tests. Consequently, a Qualisys optical measurement system (Qualisys Oqus 300+) was employed to measure sample deformation. This system operates by reflecting infrared light from six dots affixed to the sample surface, as depicted in Fig. 2(b). The dots were positioned horizontally 60 mm apart and vertically 30 mm apart from each other. Tracking the displacement of these dots in both longitudinal and lateral directions enables effective verification of the plane strain condition. The Qualisys system represents an alternative to digital image correlation, especially in cases where the deformations are large, and the shape of patterns used to track the strain change as the sample is deformed.

Each elastomer underwent testing using at least five samples to ensure robust analysis and consistent results.

Fig. 3(a) shows typical stress and strain curves for the planar tests with all five elastomers. All elastomers exhibit stable planar strain conditions reaching values higher than 200% of strain, except for SIR due to slippage after 100% of strain. All tests were stopped when slippage, elastomer failure, or debonding between the elastomer and the brackets occurred. Similar to uniaxial tests, all elastomers have a non-linear plane strain response, with SBR exhibiting the highest loading carrying capacity and stiffness.

Fig. 3(b) shows the longitudinal and transversal strains of the NR-Latex in the planar test. They were calculated based on the change in the distance between pairs of dots in the corresponding directions for the six dots as illustrated in Fig. 3(b). As can be seen, the transversal deformation is near zero as required by the plane strain condition. This was verified for all elastomers in the range of strain evaluated.

### 3.3. Biaxial test

A biaxial scissor arm fixture was developed in this work to fit with the test machine as shown in Fig. 4. As the crosshead moves, it causes the scissor arms to rotate, thereby exerting tension on the specimen at ±45° angles relative to the test machine loading direction, generating equal biaxial stress. Duncan et al. (1999) demonstrated that this fixture can uniformly distribute stresses along both principal ±45° axes, showing the reliability of the fixture for biaxial tests. Fig. 4(a) shows a schematic design of the fixture, in which "a" represents the length of one of the frame arms, "c" is the length of one of the loading arms, and "b" is the distance from the top of the fixture to the joint between the frame and the loading arms. It is important to notice that "a," "b," and "c" are constants inherent to the design of the biaxial scissor arm fixture and are 260 mm, 87 mm, and 130 mm respectively.

For the biaxial tests, samples measuring 45 mm × 45 mm were utilized, with the removal of the four corners to mitigate stress concentration, as depicted in Fig. 4(a). During the tests, a consistent 50 mm/min crosshead speed was maintained. Similar to the planar tests, sample deformation was monitored using the Qualisys optical measurement system, which tracked four dots affixed to the samples, as illustrated in Fig. 5(b).

Fig. 5(a) shows typical stress and strain curves of the biaxial tests with all five elastomers. During the tests, NBR and SIR started to slide from the grips at strain values higher than 80% causing the stoppage of the tests. The strain values in Fig. 5(a) correspond to the average between principal diagonals (diagonal 1 and diagonal 2) for each specimen and type of elastomer as shown in Fig. 5(b). Diagonals 1 and 2 are related to the distance respectively between the up-right and bottom-left reflective dots, and the up-left and bottom-right reflective dots. As can be seen from Fig. 5(b), the strain curves obtained along these two main diagonals are similar with an average difference of 9%, suggesting approximately equi-biaxial strain condition during the test. This condition was achieved for all elastomers studied in this work.

The biaxial stresses were related to the load measured by the machine using the equation introduced by Duncan et al. (1999), as shown in Equation (1), where F is the force measured by the load cell, *'D'* is the separation between diagonal grips (28 mm), and *'t'* is the specimen thickness.

$$\text{Biaxial stess} = \frac{0.354760057\ \text{F}}{D\,\text{t}} \tag{1}$$

## 4. Hyperelastic models

The data for the strain-stress response of the elastomers were used to generate the hyperelastic constants via the Abaqus hyperelastic material curve fitting tool. Based on strain-energy functions, Abaqus implements hyperelastic models and generates a set of constants to fit with the experimental data. These constants, which describe the strain-energy functions, correspond to a group that best fits all the loading modes used in the analysis, including uniaxial, planar, and biaxial curves.

Hyperelastic models are established through the definition of a strain energy function, *W,* expressed as a function of the three invariants of the Green deformation tensor defined in terms of the principal stretch ratios $\lambda_1, \lambda_2, \lambda_3$, as shown in Equations (2) and (3)

$$W = W(I_1, I_2, I_3) \tag{2}$$

**Table 1**
Principal stresses and stretches at different loading conditions.

| | Principal Stresses | Principal Stretches |
|---|---|---|
| **Uniaxial** | $\sigma_1 = \sigma$<br>$\sigma_2 = \sigma_3 = 0$ | $\lambda_1 = \lambda$<br>$\lambda_2 = \lambda_3$ |
| **Planar** | $\sigma_1 = \sigma$<br>$\sigma_2 = \sigma_2$<br>$\sigma_3 = 0$ | $\lambda_1 = \lambda$<br>$\lambda_2 = 1$ |
| **Biaxial** | $\sigma_1 = \sigma_2$<br>$\sigma_3 = 0$ | $\lambda_1 = \lambda_2$ |

$$\begin{aligned} I_1 &= {\lambda_1}^2 + {\lambda_2}^2 + {\lambda_3}^2 \\ I_2 &= {\lambda_1}^2{\lambda_2}^2 + {\lambda_2}^2{\lambda_3}^2 + {\lambda_3}^2{\lambda_1}^2 \\ I_3 &= {\lambda_1}^2{\lambda_2}^2{\lambda_3}^2 \end{aligned} \tag{3}$$

The strain-energy function integrates the principal stretches, and by using the Cauchy function, the stretches and the stresses are correlated. This enables the evaluation of material strain-stress response through Equation (4)

$$\sigma_i = \lambda_i \frac{\partial W}{\partial \lambda_i} - p \quad i = 1, 2, 3 \tag{4}$$

where $p$ represents the hydrostatic part of stress. For incompressible materials, $I_3 = 1$ and $\lambda_3$ can be expressed by $\lambda_3 = (\lambda_1\lambda_2)^{-1}$. It follows that Equation (2) can be expressed by $\lambda_1$ and $\lambda_2$ and Equation (5) can be derived from Equation (4) to eliminate the unknown hydrostatic stress:

$$\begin{aligned} \sigma_1 &= \lambda_1 \frac{\partial W}{\partial \lambda_1} \\ \sigma_2 &= \lambda_2 \frac{\partial W}{\partial \lambda_2} \end{aligned} \tag{5}$$

Depending on the loading condition, the principal stretches and stresses can be defined according to Table 1 and incorporated in Equation (3).

Once the relation between the stretches and stresses is established, the chosen hyperelastic model defines the strain-energy function. Different hyperelastic models have been assessed in this work, including Mooney-Rivlin, Ogden, Neo-Hookean, Yeoh, and Arruba-Boyce. These models provide a specific strain energy function involving the terms of $C_{ij}$ (material constant related to shear behaviour), $D_i$ (material constant related to bulk compressibility), $J_{el}$ (elastic volume ratio), and $\mu_i, \alpha_i$ (constant dependent on material properties).

Mooney–Rivlin model corresponds to a special case of the full polynomial model as shown by Equation (6) when $N$ equals 1 as in Equation (7). This model is a two-parameter phenomenological model that is adequate for describing moderately large strains during uniaxial elongation and shear deformation (Mooney, 1940; Rivlin, 1948). However, the Mooney–Rivlin model cannot accurately represent the upward curvature (S-curvature) observed in the force-extension relationship during uniaxial testing in natural rubbers, nor to describe the force-displacement relationship during shear testing.

$$\textit{Full Polynomial Model:} \quad W = \sum_{i,j=0}^{N} C_{ij}(I_1 - 3)^i (I_2 - 3)^j + \sum_{i=0}^{N} \frac{1}{D_i}(J_{el} - 1)^{2i} \tag{6}$$

$$\textit{Mooney} - \textit{Rivlin:} \quad W = C_{10}(I_1 - 3) + C_{01}(I_2 - 3) + \frac{1}{D_1}(J_{el} - 1)^2 \tag{7}$$

Unlike the full polynomial, reduced polynomial models do not include the invariant $I_2$. Removing the terms involving $I_2$ from the strain energy function, the model capability to describe the behaviour of intricate deformation states improves, especially when dealing with limited test data (Peeters et al., 1999). Neo-Hookean and Yeoh models are special cases of the reduced polynomial model.

**Table 2**
Fitting errors (%) calculated for different hyperelastic models for each elastomer.

| NR-LATEX | Mooney-Rivlin | Ogden, N3 | Neo-Hookean | Yeah | Arruda-Boyce |
|---|---|---|---|---|---|
| **Uniaxial** | 28.4 | 9.6 | 37.1 | 21.3 | 25.9 |
| **Planar** | 20.9 | 13.7 | 22.1 | 18.3 | 17.3 |
| **Biaxial** | 13.2 | 9.3 | 56.7 | 56.3 | 59.7 |
| **Average** | 20.8 | 10.9 | 38.6 | 32.0 | 34.3 |
| **Accumulative** | 62.5 | 32.6 | 115.9 | 95.9 | 102.9 |
| NR | Mooney-Rivlin | Ogden, n3 | Neo-Hookean | Yeoh | Arruda-Boyce |
| **Uniaxial** | 40.0 | 12.5 | 31.2 | 3.7 | 8.2 |
| **Planar** | 11.5 | 6.2 | 12.4 | 9.0 | 9.9 |
| **Biaxial** | 17.2 | 9.6 | 44.1 | 45.5 | 47.7 |
| **Average** | 22.9 | 9.4 | 29.2 | 19.4 | 21.9 |
| **Accumulative** | 68.7 | 28.3 | 87.6 | 58.2 | 65.8 |
| NBR | Mooney-Rivlin | Ogden, n3 | Neo-Hookean | Yeoh | Arruda-Boyce |
| **Uniaxial** | 13.2 | 9.4 | 8.2 | 6.1 | 8.2 |
| **Planar** | 8.0 | 5.3 | 7.8 | 7.3 | 7.8 |
| **Biaxial** | 18.2 | 8.7 | 32.1 | 29.2 | 32.1 |
| **Average** | 13.1 | 7.8 | 16.0 | 14.2 | 16.0 |
| **Accumulative** | 39.3 | 23.3 | 48.0 | 42.5 | 48.0 |
| SBR | Mooney-Rivlin | Ogden, n3 | Neo-Hookean | Yeoh | Arruda-Boyce |
| **Uniaxial** | 36.9 | 11.0 | 30.4 | 9.6 | 15.9 |
| **Planar** | 19.4 | 7.4 | 19.5 | 9.9 | 14.9 |
| **Biaxial** | 13.8 | 7.9 | 36.4 | 39.0 | 38.1 |
| **Average** | 23.4 | 8.8 | 28.8 | 19.5 | 22.9 |
| **Accumulative** | 70.2 | 26.3 | 86.3 | 58.5 | 68.8 |
| SIR | Mooney-Rivlin | Ogden, n3 | Neo-Hookean | Yeoh | Arruda-Boyce |
| **Uniaxial** | 21.9 | 6.8 | 20.2 | 4.0 | 6.3 |
| **Planar** | 24.1 | 13.8 | 23.9 | 16.9 | 18.9 |
| **Biaxial** | 10.7 | 5.6 | 12.5 | 16.1 | 15.5 |
| **Average** | 18.9 | 8.7 | 18.9 | 12.3 | 13.6 |
| **Accumulative** | 56.7 | 26.2 | 56.6 | 37.0 | 40.7 |

$$\textit{Reduced Polynomial Model:} \quad W = \sum_{i=0}^{N} C_{ij}(I_1 - 3)^i + \sum_{i=0}^{N} \frac{1}{D_i}(J_{el} - 1)^{2i} \tag{8}$$

Neo-Hookean constitutes a unique instance within the Mooney-Rivlin formulation, characterized by $C_{01} = 0$. This model is applicable when there is insufficient material data. Its user-friendly nature allows for effective implementation and accurate estimations, particularly for minor strains. Nevertheless, similar to previous cases, it also falls short of representing the upward curvature of the stress-strain curve.

$$\textit{Neo} - \textit{Hookean:} \quad W = C_{10}(I_1 - 3) + \frac{1}{D_1}(J_{el} - 1)^2 \tag{9}$$

Yeoh introduced a phenomenological model in the structure of a third-order polynomial that exclusively relies on the first invariant, $I_1$. This model effectively captures the stress-strain curve upward curvature. Its substantial fitting accuracy across an extensive strain spectrum permits the simulation of diverse deformation modes even with limited data availability (Renaud et al., 2009).

$$\textit{Yeoh:} \quad W = \sum_{i=0}^{3} C_{ij}(I_1 - 3)^i + \sum_{i=0}^{3} \frac{1}{D_i}(J_{el} - 1)^{2i} \tag{10}$$

Arruda-Boyce model, defined by two parameters and reliant solely on the first invariant, $I_1$, demonstrates robust performance even with limited testing data. Derived from the framework of molecular chain

**Table 3**
Hyperelastic constants of Ogden model with energy potential order 3.

| | NR-LATEX | | NR | | NBR | | SBR | | SIR | |
|---|---|---|---|---|---|---|---|---|---|---|
| I | $\mu_i$ (MPa) | $\alpha_i$ | $\mu_i$ (MPa) | $\alpha_i$ | $\mu_i$ (MPa) | $\alpha_i$ | $\mu_i$ (MPa) | $\alpha_i$ | $\mu_i$ (MPa) | $\alpha_i$ |
| **1** | 0.571 | 0.218 | 0.357 | 0.291 | −34.389 | 1.624 | −7.381 | 2.289 | 0.382 | −0.133 |
| **2** | 0.001 | 6.141 | 0.009 | 5.105 | 15.803 | 1.900 | 6.623 | 2.574 | 0.249 | 3.212 |
| **3** | 0.043 | 2.841 | 0.130 | 2.008 | 19.404 | 1.325 | 1.993 | −0.904 | 0.004 | −5.456 |

networks, this model is also known as the Arruda-Boyce 8-chain model (Arruda and Boyce, 1993).

$$Arruda-Boyce\ Model: \quad W = \mu \sum_{i=1}^{5} \frac{C_i}{\lambda_m^{2i-2}} \left(I_1^i - 3^i\right) + \frac{1}{D}\left(\frac{J_{el}^2 - 1}{2} - ln\, J_{el}\right) \tag{11}$$

Ogden model operates within the phenomenological domain and diverges from using invariants by principal stretches (Ogden, 1972a, 1972b). Notably, this model adeptly captures the stress-strain curve upward bend, effectively emulating rubber behaviour across extensive deformation ranges.

$$Ogden\ Model: \quad W = \sum_{i=0}^{N} \frac{2\mu_i}{\alpha_i^2}\left(\lambda_1^{\alpha_i} + \lambda_2^{\alpha_i} + \lambda_3^{\alpha_i} - 3\right)^i + \sum_{i=0}^{N} \frac{1}{D_i}(J_{el} - 1)^{2i} \tag{12}$$

In this study, all elastomers are considered fully incompressible. Consequently, terms in the equations that include the material constant controlling bulk compressibility, $D_i$, and the elastic volume ratio, $J_{el}$, are ignored.

Based on the experimental data obtained from three different tests, the fitting capabilities of the Mooney-Rivlin, Ogden, Neo-Hookean, Yeoh, and Arruda-Boyce models were evaluated. Table 2 presents the fitting errors calculated using Equation (13) using the stress values provided by the models and the experiments at specific strains.

$$Fitting\ Error = \frac{1}{N} \sum_{i:1}^{N} \frac{\left|\sigma_{Exp} - \sigma_{Model}\right|}{\sigma_{Exp}} \tag{13}$$

N is the total number of data points evaluated for the calculation of the fitting error, which corresponds to 41 data points along the strain-stress curve. The error was calculated based on the differences in stresses between the experimental values and the model predictions across the deformation range. Table 2 provides the fitting errors of each hyperelastic model in relation to the experimental data under different load conditions: uniaxial, planar, and biaxial. Also included in Table 2 are the error average and cumulative error across the three different loading conditions.

The Ogden model with an energy potential order of 3 emerges as the most suitable choice for predicting the behaviour of the elastomers, exhibiting the lowest average and cumulative errors among the models. As previously mentioned, the Ogden model effectively captures the upward bend of the stress-strain curve, accurately emulating rubber behaviour over a wide range of deformations. Conversely, the Neo-Hookean model exhibits the poorest fitting. Being a polynomial model with an energy potential order of 1, it is only suitable for minor strain levels and limited data. As a result, it fails to predict the upward bend observed in stress-strain curves.

Given that the Ogden model offers the most accurate curve fitting and prediction of the mechanical response of the elastomers examined in this study, Table 3 presents the hyperelastic constants employed to define Equation (12). The relation between principal stretches and stresses can then be obtained using Equation (12) and the corresponding conditions for stretches and stresses in Table 1 and Equation (4). Consequently, this enables the derivation of the strain-stress prediction curve of the Ogden model for each elastomer under different load conditions.

Fig. 6 shows the experimental curves alongside the predictions of the Ogden model using the hyperelastic constants from Table 3. The model

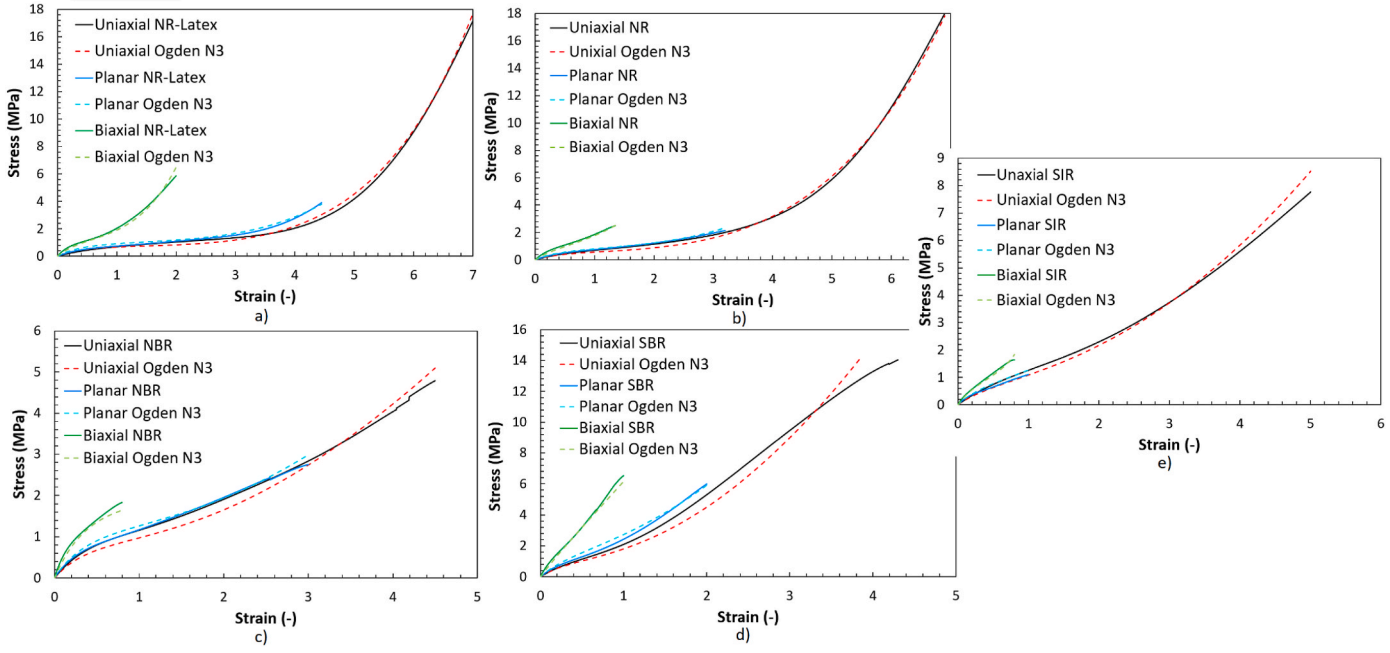


**Fig. 6.** Comparison between experimental and analytical prediction using the Ogden model, experimental curves are described in solid lines and predictions using ABAQUS are in dash lines for each elastomer respectively: (a) NR-Latex, (b) NR, (c) NBR, (d) SBR and (e) SIR.

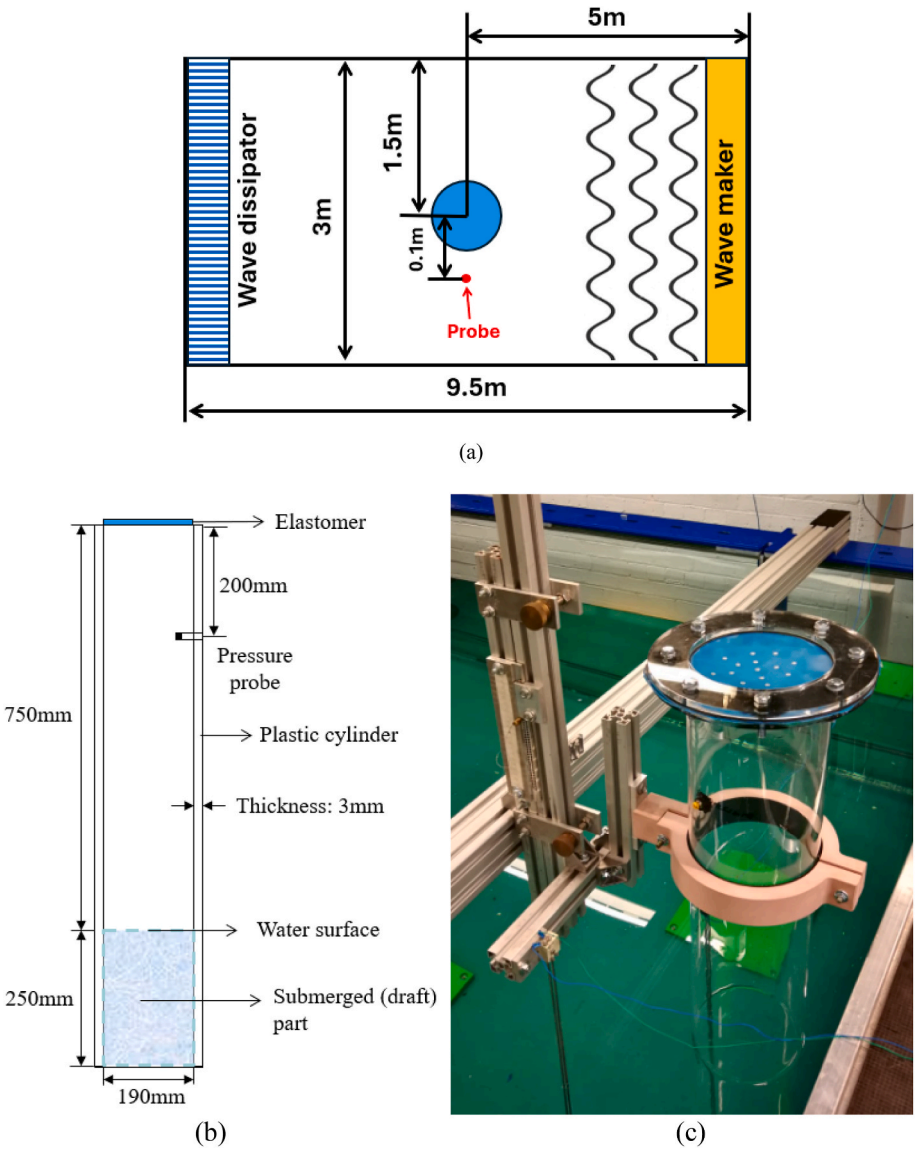


**Fig. 7.** (a) Schematic of the water tank and location of the device (b) schematic diagram of OWC and (c) photo of OWC setup in the wave tank.

demonstrates a strong agreement with the experimental curves of all five materials. In particular, an excellent agreement can be seen for NR and NR-Latex. This substantiates that the hyperelastic constants employed for the Ogden model effectively describe the mechanical response of the elastomers selected in this work.

## 5. Oscillating water column test

An oscillating water column (OWC) test was employed to validate the methodology used in this work for discerning suitable hyperelastic models in the context of fWEC. The experiment was performed in the 3D compact wave tank at the Kelvin Hydrodynamics Laboratory of the University of Strathclyde. The wave tank is equipped with 8 flap active-absorbing type wave makers, covering a wave frequency range of 0.2–2 Hz and a maximum wave height of up to 0.4m. The force-feedback active absorbing characteristic minimises the secondary reflection from the wave maker due to radiation and scattering introduced by the OWC device during testing. A set of four Wedge-type passive wave beach modules are installed the other end of the tank to dampen the incident, diffract and radiated wave, the typical reflection coefficient is less than 10%. Fig. 7 (a) shows the OWC setup in the wave tank test, where the OWC is located about the middle of the tank. For the device, the same NR-Latex characterised and modelled previously was implemented at the top. Due to its significantly lower thickness than other elastomers selected in this work, NR-Latex allowed for adequate deformations even under the limited wave amplitude generated by the wave tank. For the other materials, negligible deformations were observed with near-to-zero displacement, making them impractical for OWC analysis.

Due to the membrane low bending stiffness, a negative displacement is caused by the weight, making the material loose and wavy in its neutral position. To address this issue, the membrane was slightly pre-stretched to return it to a horizontal position. Bolts at the top periphery of the device (Fig. 7(c)) were adjusted to achieve this aim. The material is secured at these points, where the bolts pass through the acrylic lids. The bolts were tightened in a specific sequence to ensure even pressure distribution between the acrylic lids and the membrane. On the other hand, a Honeywell 163PC01D75 pressure transducer was affixed near the upper section of the cylinder to monitor air chamber pressure as indicated in Fig. 7(b). An optical measurement system, the Qualisys Oqus 300+, was positioned with two cameras above the OWC. The deformation of NF-Latex was obtained by measuring the displacement of white dots marked on the NF-Latex membrane as shown in Fig. 7 (c). During the wave tank tests, regular waves were generated with 0.01m of amplitude and 0.375 Hz of frequency.

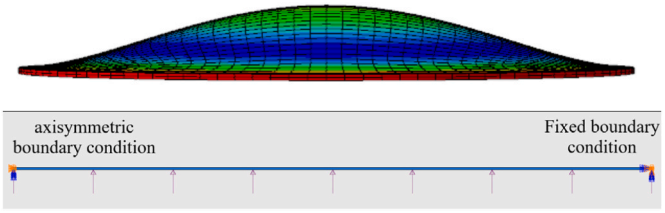


**Fig. 8.** OWC numerical model developed in Abaqus.

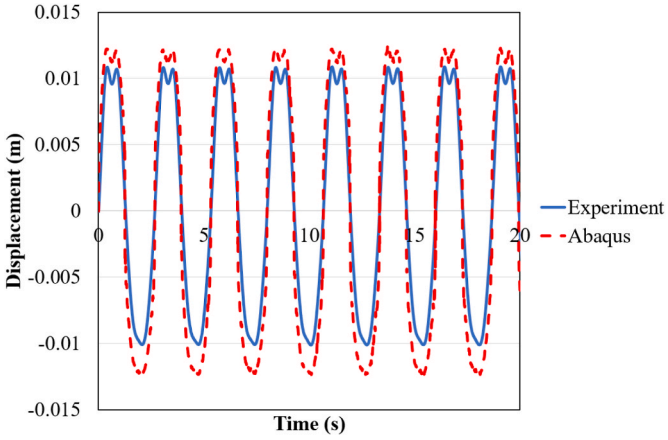


**Fig. 9.** Comparison between OWC experimental results generated using the water tank in blue solid line and the numerical model using hyperelastic constants in red dash line.

A 2D finite element model of the NF-Latex membrane was created to simulate its displacement during the wave tank tests as shown in Fig. 8. The hyperelastic constants derived for the NR-Latex in Table 3 were used to define the material behaviour. The elastomer was represented using bilinear axisymmetric quadrilateral elements with 4-node (CAX4H). Data obtained from the pressure transducer were used as the loading condition.

Fig. 9 presents a comparison of the results for the longitudinal displacement of the NF-Latex membrane between the simulation and the experimental data acquired from the wave tank test. It can be seen that the applied hyperelastic model is capable of following the deformation trend of the flexible membrane. However, a slight discrepancy exists in the maximum and minimum displacements between the experimental and the numerical model. This difference may result from various factors that cumulatively increase the divergence between the numerical and OWC experimental results. Among these factors are errors introduced during material characterization, data collection, and post-processing; fitting errors of the hyperelastic models listed in Table 2; uncertainties in the measurement equipment, including the tensile test machine, Qualisys system, and pressure transducer; and the pre-stretching applied to the NF-Latex membrane during the OWC setup. While this pre-stretching prevents the material from becoming loose during unloading conditions, it also makes the material behave stiffer, leading to lower displacement of the membrane during the test.

## 6. Conclusions

Several commercial elastomers were characterised under multiple loading conditions and their corresponding stress and strain behaviour was subsequently modelled by hyperelastic models. The results suggested that the Ogden model, with an energy potential order of 3, provided a better fit across all elastomers studied in this work. The hyperelastic constants and the methodology developed in this work were successfully applied to one of the elastomers used as a flexible membrane in an oscillating water column test. The modelled membrane showed good agreement with the experimental results obtained from the wave tank test with an accuracy of 85% in displacement. The discrepancy was found to be caused by different accumulative error sources listed before including the pre-stretching applied to the flexible membrane during its installation in the test rig. Nevertheless, this study has demonstrated a promising methodology for analysing flexible materials, such as typical elastomers, used in wave energy converters.

## CRediT authorship contribution statement

**Guillermo Idarraga:** Writing – review & editing, Writing – original draft, Visualization, Validation, Software, Methodology, Investigation, Formal analysis, Data curation, Conceptualization. **Liu Yang:** Writing – review & editing, Writing – original draft, Visualization, Validation, Supervision, Software, Resources, Methodology, Investigation, Funding acquisition, Formal analysis, Data curation, Conceptualization. **Farhad Abad:** Writing – review & editing, Validation, Investigation, Data curation. **Yang Huang:** Writing – review & editing, Validation, Investigation, Data curation. **Saishuai Dai:** Writing – review & editing, Validation, Methodology, Investigation, Data curation. **Qing Xiao:** Writing – review & editing, Validation, Supervision, Project administration, Funding acquisition, Data curation. **Saeid Lotfian:** Investigation, Conceptualization. **Feargal Brennan:** Supervision, Project administration, Investigation, Funding acquisition.

## Declaration of competing interest

The authors declare that they have no known competing financial interests or personal relationships that could have appeared to influence the work reported in this paper.

## Acknowledgement

This research was supported by an Engineering and Physical Sciences Research Council (EPSRC) Grant “Bionic Adaptive Stretchable Materials for WEC (BASM-WEC)” (No. EP/V040553/1). This work used the Cirrus UK National Tier-2 HPC Service at EPCC (http://cirrus.ac.uk) funded by the University of Edinburgh and EPSRC (No. EP/P020267/1).

## References

Aderinto, T., Li, H., 2018. Ocean wave energy converters: Status and challenges. Energies 11 (5), 1250. https://doi.org/10.3390/en11051250.

Ahamed, R., McKee, K., Howard, I., 2020. Advancements of wave energy converters based on power take off (PTO) systems: a review. Ocean Eng. 204, 107248. https://doi.org/10.1016/j.oceaneng.2020.107248.

Alam, M.R., 2012. A flexible seafloor carpet for high-performance wave energy extraction. Proceedings of OMAE 2012. 31st International Conference on Ocean. Offshore and Arctic Engineering, Rio de Janeiro, Brazil. https://doi.org/10.1115/OMAE2012-84034.

Arruda, E.M., Boyce, M.C., 1993. A three-dimensional constitutive model for the large stretch behaviour of rubber elastic materials. J. Mech. Phys. Solid. 41 (2), 389–412. https://doi.org/10.1016/0022-5096(93)90013-6.

Babarit, A., et al., 2017. Investigation on the energy absorption performance of a fixed-bottom pressure-differential wave energy converter. Appl. Ocean Res. 65, 90–101. https://doi.org/10.1016/j.apor.2017.03.017.

Bojek, P., Bahar, H., 2021. Renewable Power – Report. International Energy Agency (IEA).

Chaplin, J.R., et al., 2012. Laboratory testing the anaconda. Phil. Trans. R. Soc. A 370, 403–424. https://doi.org/10.1098/rsta.2011.0256.

Collins, I., 2021. Flexible membrane structures for wave energy harvesting: a review of the developments, materials and computational modelling approaches. Renew. Sustain. Energy Rev. 151, 111478. https://doi.org/10.1016/j.rser.2021.111478.

Duncan, B.C., et al., 1999. Verification of Hyperelastic Test Methods. Teddington: NPL. NPL Report CMMT(A) 226.

Jean, P., et al., 2012. Standing wave tube electro active polymer wave energy converter. Proc. SPIE 8340, 83400C. https://doi.org/10.1117/12.934222, 1.

Kaltseis, R., et al., 2014. Natural rubber for sustainable high-power electrical energy generation. RSC Adv. 4 (53), 27 905–927 913. https://doi.org/10.1039/C4RA03090G.

K. Koca, et al. Recent advances in the development of wave energy converters. The 10th European Wave and Tidal Energy Conference (EWTEC 2013), Aalborg, Denmark.

Kurniawan, A., et al., 2017. Wave energy absorption by a floating air bag. J. Fluid Mech. 812 (10), 294–320. https://doi.org/10.1017/jfm.2016.811.
Li, X., et al., 2021. Dynamic response of a novel flexible wave energy converter under regular waves. Proceedings of the 14th European Wave and Tidal Energy Conference 5-9th Sept. Plymouth, UK.
Lin, Y., et al., 2015. Review of hydraulic transmission technologies for wave power generation. Renew. Sustain. Energy Rev. 50, 194–203. https://doi.org/10.1016/j.rser.2015.04.141.
Lindquist, H., 2017. The journey of reinventing the European electricity landscape. In: Renewable Energy Integration. Elsevier, pp. 3–13. https://doi.org/10.1016/B978-0-12-809592-8.00001-9.
Maas, J., Graf, C., 2012. Dielectric elastomers for hydro power harvesting. Smart Mater. Struct. 21 (12pp), 064006. https://doi.org/10.1088/0964-1726/21/6/064006.
Materials Landscaping Study – Final Report. WES_LS01_ER_Materials.
McDonald, A., et al., 2019. Linear analysis of fluid-filled membrane structures using generalised modes. Proceedings of the 13th European Wave and Tidal Energy Conference 1-6th Sept. Naples, Italy.
Mooney, M.A., 1940. A theory of large elastic deformation. J. Appl. Phys. 11 (9), 582–592. https://doi.org/10.1063/1.1712836.
Moretti, G., et al., 2019. Modelling and testing of a wave energy converter based on dielectric elastomer generators. Proc. R. Soc. A 475, 20180566. https://doi.org/10.1098/rspa.2018.0566.
Moretti, G., et al., 2020. Advances in the development of dielectric elastomer generators for wave energy conversion. Renew. Sustain. Energy Rev. 117, 109430. https://doi.org/10.1016/j.rser.2019.109430.
Ogden, R.W., 1972a. Large deformation isotropic elasticity— on the correlation of theory and experiment for the incompressiblerubberlike solids. Proc. Roy. Soc. Lond. Series A, Math. Phys. Sci. 326 (1567), 565–584. https://doi.org/10.1098/rspa.1972.0026.
Ogden, R.W., 1972b. Large deformation isotropic elasticity—on the correlation of theory and experiment for the compressible rubberlike solids. Proc. Roy. Soc. Lond. 328 (1575), 567–583. https://doi.org/10.1098/rspa.1972.0096.
Orphin, J., Fleming, A., Algie, C., 2017. Physical scale model testing of a flexible membrane wave energy converter: videogrammetric analysis of membrane operation. International Journal of Marine Energy 20, 135–150. https://doi.org/10.1016/j.ijome.2017.09.004.
Peeters, F.J.H., Kussner, M., 1999. Material law selection in finite element simulation of rubber-like materials and its practical application in the industrial design process. In: Dorfmann, A., Muhr, A. (Eds.), Constitutive Models for Rubber. A. A. Balkema Publishers, Rotterdam, pp. 29–36.
PolyWEC project. Final Publishable Summary Report. Grant Agreement number: 309139.
Renaud, C., et al., 2009. The Yeoh model applied to the modeling of large deformation contact/impact problems. Int. J. Impact Eng. 36 (5), 659–666. https://doi.org/10.1016/j.ijimpeng.2008.09.008.
Righi, M., et al., 2021. A broadbanded pressure differential wave energy converter based on dielectric elastomer generators. Nonlinear Dyn 105, 2861–2876. https://doi.org/10.1007/s11071-021-06721-8.
Rivlin, R.S., 1948. Large elastic deformations of isotropic materials I: fundamental concepts. Phil. Trans. Roy. Soc. Lond. A 240 (822), 459–490. https://doi.org/10.1098/rsta.1948.0002.
Seanergy. Ocean Energies, 2016. Moving towards Competitiveness: a Market Overview.
Technology Description and Status Electric Eel. Knowledge Capture Project, AWS Project No 15-007.
Yemm, R., et al., 2012. Pelamis: experience from concept to connection. Phil Trans R Soc A 370, 365–380. https://doi.org/10.1098/rsta.2011.0312, 1959.